Beyond Static Geometries: A Novel Dynamic 3D Hemodynamic Model of Left Atrium for Personalized Cardiovascular Risk Assessment

João Lameu[1], João G. B. Torro[1], Rodrigo L. Amaral[1]

[1]Federal University of ABC, São Bernardo do Campo, Brazil

Abstract

Left ventricular diastolic dysfunction (DD), affecting 25-30% of the general elderly population, significantly elevates cardiovascular risk by impairing left atrium (LA) mechanics, ventricular filling and deprecating atrial ejection fractions. DD progresses through three stages: altered relaxation, pseudonormal, and restrictive filling patterns, each associated with worsening atrial dysfunction and elevated thrombotic risk. We developed a novel computational approach using dynamic LA volume changes derived from clinical phasic volumes. This method enables a comprehensive evaluation of LA mechanical performance and high-resolution 3D hemodynamics, including thrombogenic risk assessment, across diverse clinical scenarios. A single 3D LA model, acquired at end-systole, served as the geometric basis for generating N volume-varying meshes spanning the entire cardiac cycle during pre-processing. The meshes were dynamically deformed in the 3D hemodynamic model, according to reservoir, conduit and booster pump phases, incorporating mitral valve closure effects. Three scenarios were evaluated: (1) a healthy case (dynamic model), (2) pseudonormal DD (dynamic model), (3) pseudonormal DD (static model). Numerical results showed organized vortical flow with physiological protective Time-Averaged Wall Shear Stress (TAWSS) (>1 Pa) in healthy subjects versus increased stasis, marked by low TAWSS (<0.1 Pa) and blood stagnation in left atrial appendage (LAA) in pseudonormal scenarios. The dynamic model demonstrated superior LAA washout compared to the static model, particularly in the healthy case, attributed to the preserved ejection fraction. This clinically translatable framework enables personalized risk assessment using routine clinical data, bridging the gap between complex imaging techniques and potential hemodynamic evaluation without requiring costly simulations or dynamic LA reconstruction.

1. Introduction

Left ventricular diastolic dysfunction (DD) affects 25-30% of community-based populations, with higher prevalence in elderly patients and those with hypertension, diabetes, or chronic kidney disease [1]. This progressive condition impairs ventricular filling, elevates intracardiac pressures [2,3], and disrupts left atrial mechanics and hemodynamics. DD progresses through three stages: altered relaxation (Type I), pseudonormal (Type II), and restrictive (Type III) patterns [3,4], each progressively compromising atrial volumes and ejection fractions while heightening thrombogenic risk [3-6]. The left atrial volume index (LAVI) serves as a key biomarker, with values >34 mL/m² indicating significant dilation [7]. Phasic LAVI enable calculation of passive, active, and total ejection fractions of LA, crucial for risk stratification in arrhythmias and DD [5,6,8,9]. Clinical observations reveal progressive LAVI increases and LA ejection fraction reductions with DD severity, particularly affecting active ejection fraction and correlating with atrial fibrillation onset [5].

Despite advances in understanding LA mechanics and their relationship with disease progression, a high-resolution hemodynamic assessment under DD conditions remains underexplored, particularly in terms of 3D volume dynamics and thrombotic risk quantification. While Computational Fluid Dynamics (CFD) enables detailed LA flow analysis, most models neglect dynamic volume changes and mitral valve effects [10-12]. This study introduces a clinically accessible CFD approach incorporating dynamic volume variations based on phasic volumes (maximum, at end-systole, V_{max}; pre-atrial contraction, $V_{pre\text{-}A}$; minimum, V_{min}), closed mitral valve effects, and pulsatile flow profiles to improve thrombotic risk stratification in DD patients.

2. Mathematical Modeling

The proposed model uses a 3D LA geometry, obtainted from public dataset [9], acquired at end-systole to generate the base mesh. During preprocessing, *N* meshes with varying volumes were generated, by isotropic scaling of the base mesh to represent the cardiac cycle phases: reservoir, conduit, and active contraction (booster pump, BP) [10]. The meshes were dynamically deformed during simulation according to the cycle phase, using Events functionality of Ansys Fluent Solver, as illustrated

in Figure 1-a. The approach incorporated closed mitral valve effects during reservoir phase. Cardiac cycle meshes were dynamically adjusted at 1 mL volume intervals, though the method accommodates arbitrary resolution based on required detail levels. The phasic volumes - V_{min}, V_{max} and $V_{pre\text{-}A}$ (Figure 1-a) - obtained from clinical data ware summarized in Table 1. These volumes quantified LA volume rate change per atrial cycle phase, defining the dynamic mesh model (Figure 1-b, green lines). In Table 1, *p-LAEF* (%) = $100\cdot[(V_{max} - V_{pre,A})/V_{max}]$, *a-LAEF* (%) =$100\cdot[(V_{pre,A} - V_{min})/V_{min}]$ and *LAEF* (%) = $100\cdot[(V_{max} - V_{min})/V_{max}]$ are the passive, active and total left atrium ejection fraction.

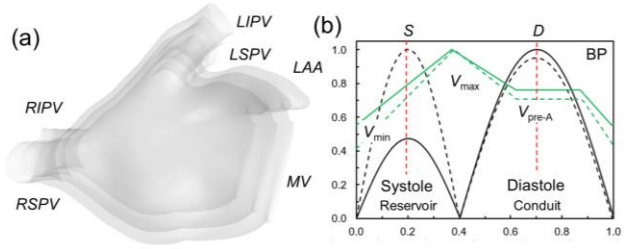

Figure 1. (a) Superposition of three surfaces of LA at phasic volumes with anatomical markers (R, L – right, left; I, S – inferior, superior, PV – pulmonary vein, MV – mitral valve, LAA – left atrial appendage; (b) Normalized profiles of flow rate (black lines) with *S* and *D* peaks, along the LA phases (BP is the booster pump), and LA volume (green lines) with details of phasic volumes.

Table 1. Clinical parameters for LA phasic volume and ejection fractions for dynamic model [5,7,8,10]. The static model used only V_{max}.

Clinical parameter	Healthy	Pseudonormal (DDII)
$LAVI_{max}$ (mL/m^2)	29	48
V_{min} (mL)	24	53
V_{max} (mL)	58	96
$V_{pre\text{-}A}$ (mL)	41	73
p-LAEF (%)	29	24
a-LAEF (%)	42	27
LAEF (%)	59	45

Phasic volumes were obtained from clinical data of LAVI considering a Body Surface Area of 2.0 m² [7].

The Ansys CFD package was employed in all steps, from 3D geometry preparation (Ansys SpaceClaim), mesh generation (Ansys Meshing) to the numerical solution (Ansys Fluent) and post-processing (Ansys CFD-Post). The base geometry was used to generate hybrid-element meshes with about 1.8 million cells. In wall-zones, 10 inflation layers were generated (first layer thickness of 0.01 mm, growth rate of 1.2) for accurate velocity gradient estimations. The main characteristics of the model were: laminar, isothermal, incompressible, transient/pulsatile flow, with non-Newtonian blood behaviour (Carreau-Yasuda model) [11].

Pulmonary vein (PV) inflow was modelled using clinically-derived pulsatile profiles [4], featuring systolic (*S*) and diastolic (*D*) peaks. Healthy cases used $S/D = 1.0$, while DDII used $S/D \approx 0.5$ [4]. Cardiac output was set to ~5 L/min at 75 bpm (cycle duration T = 0.8 s). In dynamic models, the mitral valve closed during reservoir phase (open otherwise) with 8 mmHg outlet pressure [13]. The static model (rigid mesh) maintained an open valve throughout the cardiac cycle at constant 8 mmHg [13]. Three scenarios were evaluated: (1) healthy case with dynamic model, (2) pseudonormal DD (Type II) with dynamic model, and (3) pseudonormal DD with a rigid mesh (static approach).

For the numerical solution, a residual target (RMS) of 1×10^{-4} was employed. Two complete cardiac cycles were simulated using a time step of 1×10^{-3} s, and time-averaged values were obtained for the last cycle. The thrombus-prone regions were assessed by blood stasis zones, i.e., low blood velocities, usually below 10 cm/s [14] and the Time-Averaged Wall Shear Stress (*TAWSS*), with the thromboembolic risk classified as: high risk for *TAWSS* < 0.1 Pa, low risk for *TAWSS* > 0.4 Pa [13,15]. For the dynamic models, the time-averaged values were obtained for the mean LA volume along the cardiac cycle.

3. Results and Discussion

Figure 2(i-iii) presents the instantaneous results for velocity fields at systolic peak, diastolic peak and end-diastole (onset of atrial contraction), alongside time-averaged velocity (Figure 2-iv). Figure 2(v-vi) demonstrates two perspective views of the *TAWSS* field on LA surface. In the healthy case with a dynamic mesh (Figure 2-a), ventricular systole shows blood inflow from the PVs filling the entire atrial chamber, including the LAA, accompanied by a prominent vortical flow in the LA. This organized pattern mitigates stasis and optimizes LA filling [16,17]. The dynamic model accounted for LA expansion and gradual pressure rise during filling, yielding a more realistic hemodynamic pattern [18]. In pseudonormal DD (Type II) elevated LA pressure compensates for impaired ventricular relaxation, significantly altering hemodynamics (Figure 2-b). Compared to the healthy case (Figure 2-a), blood stagnation predominated throughout the LA chamber, attributed to LA dilation and absence of vortical flow patterns (Figure 2-b). PV inflow jets also exhibited lower velocities, consistent with larger cross section areas, consistent with clinical observations [19]. For the static DDII model (Figure 2-c), continuous mitral outflow produced near-uniform velocity field with pronounced LAA stagnation. Rigid-wall simulations overestimate thrombotic risk by neglecting atrial deformation's impact on stasis [12,15].

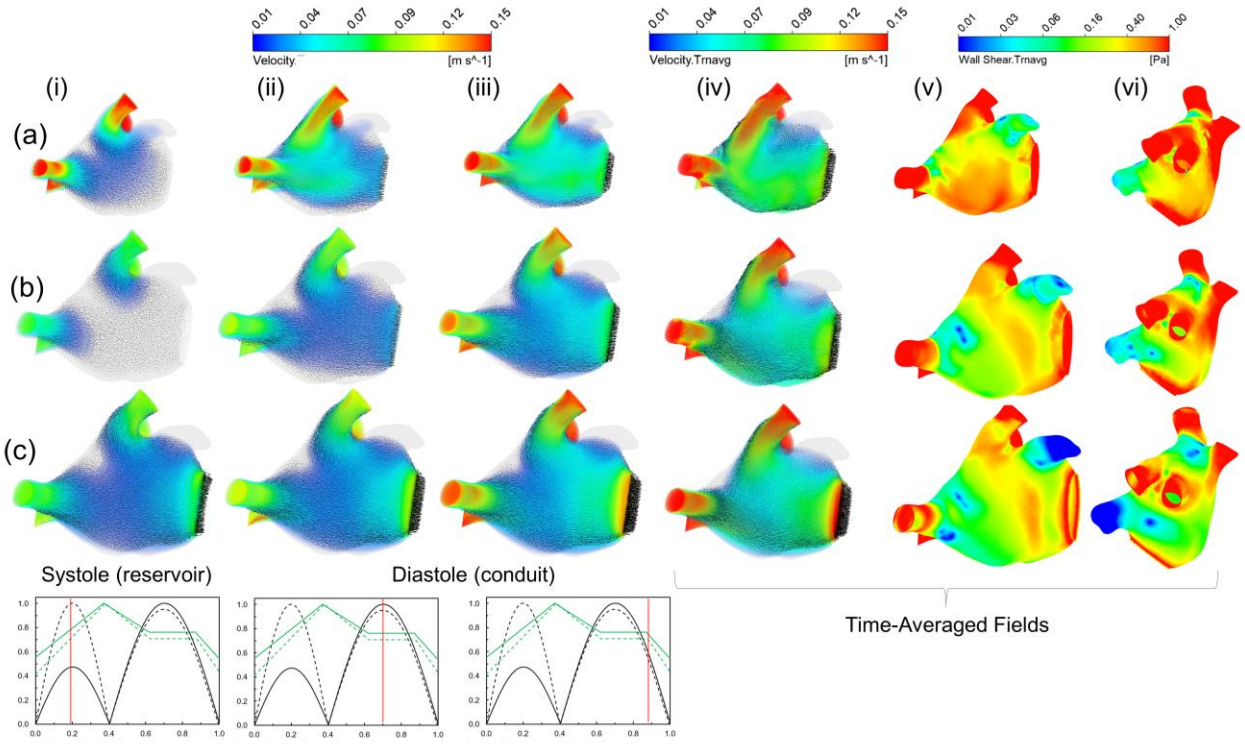

Figure 2. (a) Healthy dynamic model, (b) DDII dynamic model; (c) DDII static model. (i)-(iii) Instantaneous velocity fields at (i) systolic peak, (ii) diastolic peak and (iii) diastolic end; (iv-vi) time-averaged fields for (iv) velocity and (v-vi) *TAWSS* for two perspective view of LA surface.

The conduit phase (open mitral valve) enables passive PV-to-ventricle flow during early diastole. The LA acts as a conduit, directing flow efficiently to the mitral annulus [16,17], as seen in both dynamic models (Healthy, Figure 2-a; DDII, Figure 2-b). The healthy case maintained the vortical pattern initiated during systole, driven by left PV inflow, while right PV flow traversed the vortex periphery. This mechanism prevents stasis and enhances LAA washout – markedly diminished in DDII [16,17]. Declining LA pressure during ventricular filling maintained streamlined flow with minimal stasis [16,17]. Healthy cases exhibited higher velocities owing to smaller volumes versus DDII [16,17]. Although dynamic and rigid models shared similar conduit-phase patterns in the main chamber, DDII cases showed LAA stagnation from direct mitral flow, exacerbated by chamber enlargement. The superior active ejection fraction in healthy dynamic models reduced LAA stagnation, validated by *TAWSS* distributions (Figure 2-v-vi). Smaller LA volumes promote distinct intra-atrial vortices, whereas larger volumes disrupt them (Figure 2-b,c) [20,21]. Vortices improve PV-to-MV transit efficiency [21], their disruption in DDII elevates stasis and thrombogenic risk – particularly in the LAA – due to impaired washout from reduced active/total ejection fractions [20,21] (Figures 2-b,c). At cycle end, the healthy dynamic case achieved higher global time-averaged velocity, attributed to smaller atrial volume [20,21], whereas static DDII showed higher transmitral velocity but lower global velocity, producing larger stasis zones consistent with *TAWSS* analysis (Figure 3).

The *TAWSS* distribution at LA surface (Figure 3) revealed distinct patterns. The healthy dynamic model demonstrated higher, physiological protective *TAWSS* (> 1.0 Pa) throughout the atrial chamber, reflecting lower thromboembolic risk due to higher blood velocities and ejection fractions and smaller LA volume. For DDII cases, low-shear regions appeared in the upper atrium zone between opposite PVs, which can be attributed to flow jet interactions and chamber dilation. Very low *TAWSS* (< 0.1 Pa) were also noticed in LAA, particularly at its apex in dynamic models - a known thrombogenic site in arrhythmias and cardiac dysfunction [11,22]. The static DDII model exhibited extensive low-*TAWSS* areas (< 0.1 Pa) covering over half the appendage length (from apex to ostium) and significantly larger stasis zones compared to dynamic models. This can be attributed to lower LAA velocities inherent from the absent active ejection.

4. Conclusion

This study demonstrated that our clinically accessible CFD framework incorporating dynamic volume variations parameterized by phasic volumes, mitral valve closure effects, and pulsatile flow profiles, enabling

effective hemodynamic discrimination of thrombotic risk in DD patients. In healthy case, dynamic modelling demonstrated efficient LA filling with organized vortical flow. minimizing stasis, maintaining physiological protective *TAWSS*. Pseudonormal DD (Type II) cases exhibited larger volumes disrupting vortex formation, with extended low-velocity zones and elevated LAA stagnation. The dynamic model quantified active ejection effects, revealing reduced LAA stasis and volume-dependent *TAWSS* distributions corresponding to clinical thrombotic sites, along with conduit-phase efficiency impairment in DDII. By integrating routine clinical parameters with hemodynamic simulation, this framework provides a practical tool for risk stratification by *TAWSS* mapping and disease monitoring by accounting for the LA remodelling progression. Future work should evaluate and validate the results in larger cohort of patient-specific geometries while maintaining the computational efficiency of the proposed dynamic approach.

Acknowledgement

This study was financed in part by the Coordenação de Aperfeiçoamento de Pessoal de Nível Superior - Brasil (CAPES) - Finance Code 001. The authors thank the financial support by CNPq (National Council for Scientific and Technological Development, Process 405055/2023-4).

Conflict of Interest

The authors declare do not have conflict of interest

References

[1] J. Levene, et al., "Patient Outcomes by Ventricular Systolic and Diastolic Function," J. Am. Heart Assoc., vol. 13, no. 4, p. e033211, Feb. 2024.

[2] R.-N. Horodinschi and C. C. Diaconu, "Heart Failure and Atrial Fibrillation: Diastolic Function Differences Depending on Left Ventricle Ejection Fraction," Diagnostics, vol. 12, no. 7, p. 839, 2022.

[3] L. Darwin, et al., "Diastolic dysfunction and atrial fibrillation in coronary heart disease surgery: A literature review," IJS Open, vol. 55, p. 100615, 2023.

[4] G. C. Fernández-Pérez, R. Duarte, M. Corral de la Calle et al., "Analysis of left ventricular diastolic function using magnetic resonance imaging," Radiologia, vol. 54, no. 4, pp. 295–305, 2012.

[5] A. Singh et al., "LA Strain for Categorization of LV Diastolic Dysfunction," JACC: Cardiovasc. Imag., vol. 10, no. 7, pp. 735–743, 2017.

[6] M. Habibi et al., "Left Atrial Mechanical Function and Incident Ischemic Cerebrovascular Events Independent of AF: Insights from the MESA Study," JACC: Cardiovasc. Imag., vol. 12, no. 12, pp. 2417–2427, 2019.

[7] B. D. Hoit, "Left Atrial Size and Function: Role in Prognosis," J. Am. Coll. Cardiol., vol. 63, no. 6, pp. 493–505, 2014.

[8] M. L. Mojica-Pisciotti et al., "Left atrium phasic impairments in paroxysmal atrial fibrillation patients assessed by cardiovascular magnetic resonance feature tracking," Sci. Rep., vol. 12, p. 7539, 2022.

[9] C. H. Roney, et al., "Predicting Atrial Fibrillation Recurrence by Combining Population Data and Virtual Cohorts of Patient-Specific Left Atrial Models," Circ. Arrhythm. Electrophysiol., vol. 15, no. 2, p. e010253, 2022.

[10] A. Demirkiran, et al., "Altered left atrial 4D flow characteristics in patients with paroxysmal atrial fibrillation in the absence of apparent remodeling," Sci. Rep., vol. 11, no. 1, 2021.

[11] G. M. Bosi et al., "Computational Fluid Dynamic Analysis of the Left Atrial Appendage to Predict Thrombosis Risk," Front. Cardiovasc. Med., vol. 5, p. 34, 2018.

[12] J. Lameu, et al., "Thrombogenesis and Hemodynamic in Left Atrium Under Atrial Fibrilation," in Proc. Comput. Cardiol., Tampere, Finland, 2022, pp. 1–4.

[13] J. Mill, et al., "Sensitivity Analysis of In Silico Fluid Simulations to Predict Thrombus Formation after Left Atrial Appendage Occlusion," Mathematics, vol. 9, no. 18, p. 2304, 2021.

[14] M. Nakaza, et al., "Dual-VENC 4D Flow MRI Can Detect Abnormal Blood Flow in the Left Atrium That Potentially Causes Thrombosis Formation after Left Upper Lobectomy," Magn. Reson. Med. Sci., vol. 21, pp. 433–443, 2021.

[15] C. Albors, et al., "Impact of occluder device configurations in in-silico left atrial hemodynamics for the analysis of device-related thrombus," PLoS Comput. Biol., vol. 20, no. 9, p. e1011546, Sep. 2024.

[16] V. Vedula, et al., "Hemodynamics in the Left Atrium and Its Effect on Ventricular Flow Patterns," J. Biomech. Eng., vol. 137, no. 11, p. 111003, 2015.

[17] A. Fyrenius, et al., "Three dimensional flow in the human left atrium," Heart, vol. 86, no. 4, pp. 448–455, 2001.

[18] X. Liu, et al., "LAFlowNet: A dynamic graph method for the prediction of velocity and pressure fields in left atrium and left atrial appendage," Eng. Appl. Artif. Intell., vol. 136, p. 108896, 2024.

[19] T. Ishizu, et al., "The Wake of a Large Vortex Is Associated with Intraventricular Filling Delay in Impaired Left Ventricles with a Pseudonormalized Transmitral Flow Pattern," Echocardiography, vol. 23, no. 9, 2006.

[20] T. Saitoh, et al., "Analyses of intra-left atrial vortex and flow dynamics from pulmonary veins to left ventricle using phase-resolved three-dimensional cine contrast Magnetic Resonance Imaging (4D-Flow MRI)," Eur. Heart J., vol. 34, p. 2938, 2013.

[21] K. Suwa, et al., "Characteristics of intra-left atrial flow dynamics and factors affecting formation of the vortex flow -- analysis with phase-resolved 3-dimensional cine phase contrast magnetic resonance imaging," Circ. J., vol. 79, no. 1, pp. 144–152, 2014.

[22] N. M. Al-Saady, O. A. Obel, and A. J. Camm, "Left atrial appendage: structure, function, and role in thromboembolism," Heart, vol. 82, no. 5, pp. 547–554, 1999.

João Lameu da Silva Jr.
Federal University of ABC (UFABC)
Alameda da Universidade, s/n, São Bernardo do Campo, Brazil
joao.lameu@ufabc.edu.br